Investigation of a Monotropic Liquid Crystal Polyurethane Based on Biphenol, 2,6-Tolylene Diisocyanate, and a Six Methylene Containing Flexible Spacer. 2. IR Spectroscopic Phase Characterization

Fotios Papadimitrakopoulos, Eiji Sawa,† and William J. MacKnight*

Department of Polymer Science and Engineering, University of Massachusetts, Amherst, Massachusetts 01003

Received March 2, 1992

ABSTRACT: The mesophase to crystal phase transition observed upon heating the monotropic liquid crystal polyurethane (2,6-LCPU-6), based on the mesogenic biphenol 4,4′-bis(6-hydroxyhexoxy)biphenyl (BHHBP) and 2,6-tolylene diisocyanate (2,6-TDI), has been investigated by differential scanning calorimetry (DSC), wide-angle X-ray scattering (WAXS), and infrared (IR) spectroscopy. Hexafluoroisopropyl alcohol (HFIP) fast solvent-evaporation casting resulted in 2,6-LCPU-6 thin films with a glassy mesophase morphology. The mesophase to crystal exothermic transition has been observed by DSC between 130 and 140 °C, depending on sample preparation. It is accompanied by a substantial increase of H-bonding between urethane C=O and NH, as observed by IR. Curve-fitting analysis of the conformationally sensitive amide I region revealed three bands: ordered H-bonded carbonyl groups, disordered H-bonded carbonyl groups, and "free" carbonyl groups. The prime feature of the 130 °C transition is the substantial increase of ordered H-bonded carbonyl groups at the expense of disordered H-bonded carbonyl groups. Crystal melting occurs between 180 and 210 °C and is accompanied by the complete disappearance of the ordered H-bonded peak along with substantial changes in the frequency and width at half-height of the disordered H-bonded peak.

Introduction

In the previous paper of this series,[1] the phase behavior of the thermotropic liquid crystal polyurethane poly(4,4′-bis(6-hydroxyhexoxy)biphenyl-2,6-tolylene diisocyanate) (2,6-LCPU-6) was examined with emphasis on the mesophase structure characterization. Detailed thermal, wide-angle X-ray scattering (WAXS), and optical microscopy investigations have shown that 2,6-LCPU-6 is a monotropic[2-4] liquid crystalline polymer, with its isotropic to mesophase transition 60–70 °C lower than the crystal melting transition. One of the most striking characteristics of this polymer is the rapid crystallization of the vitrified mesophase upon heating,[1] which occurs 50–60 °C lower than the crystal melting transition.

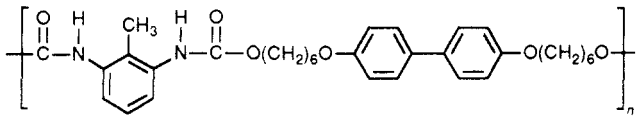

2,6-LCPU-6

While the microstructural changes and dynamics that govern enantiotropic[2-4] liquid crystal phase behavior have been active and growing areas of study among the scientific community,[5-13] comparatively little attention has been paid to monotropic liquid crystals. This arises from the absence of the traditional crystal to mesophase transition observed in enantiotropic liquid crystals, making them easily amenable to such studies. In the case of 2,6-LCPU-6, heating the vitrified mesophase above its melting point results in a well-defined mesophase to crystal transition, just the reverse of the enantiotropic case. Therefore, it can be treated in a fashion[1,14] similar to the transition in enantiotropic liquid crystal polymers.

Vibrational spectroscopy is one of the principal techniques for examining chain–chain interactions and conformational order in polymers[15-19] and their temperature dependencies. Provided that band overlapping does not occur, the various functional groups in the chemical repeat unit of 2,6-LCPU-6 can yield useful information about the degree of conformational order,[19,20] the degree of self-association in the urethane moieties,[21-24] and other intra- and intermolecular interactions of rigid aromatic units.[15] Yang et al.[7] using specifically labeled partially-deuterium-substituted molecules were able to determine the extent to which the disordering of aliphatic chains contributes to the overall entropy of phase transitions compared to the contribution of rigid aromatic groups in discotic liquid crystalline systems. The strong and specific hydrogen-bonding interactions in polyurethane systems led to infrared bands sensitive to chain packing. Lee et al.[25] utilized this observation to determine the degree of phase separation in segmented polyurethane elastomers.

The polyurethane used in this study (2,6-LCPU-6) as well as the isomeric 2,4-LCPU-6 (condensation product of 2,4-TDI and the mesogenic diol BHHBP[5]) provides three regular alternating moieties, based on different functionalities.[26-28] The rigid biphenol units and TDI moieties may be used to probe the contribution of the intermolecular forces that lead to the ordering of the liquid crystalline and crystalline phases.[15] On the other hand, the hexamethylene sequence may provide a measure of the intramolecular disorder through the trans–gauche ratio[5,15,19,20] present in it. With the combination of vibrational spectroscopy which provides a measure of the localized structure, along with DSC, WAXS, and optical microscopic measurements (which examine the long-range order of the sample), we hope to provide a better understanding of the microstructural changes occurring in the different phases.

The present paper is a continuation of the vibrational spectroscopic investigation of mesogen-containing polyurethanes. Previous efforts by Pollack et al.[26,28] and by Shen et al.[27] on the 2,4-LCPU-6 did not address all the microstructural changes occurring in the different phases. The reason for this lies in the structure of 2,4-LCPU-6. The random placement of the methyl group along the

* To whom correspondence should be addressed.
† Present address: Bridgestone Corp., Tokyo, Japan.

0024-9297/92/2225-4682$03.00/0

polymer backbone results in slower crystallization of the vitrified mesophase upon thermal treatment than is the case with 2,6-LCPU-6. This leads to a coexistence of both the mesophase and crystal state, complicating the interpretation. 2,6-LCPU-6 with its highly regular structure and sharp crystallization from the vitrified mesophase does not present the above problems.

Experimental Section

Materials. The synthesis of 2,6-LCPU-6 has been described elsewhere.[1] In this study, all of the 2,6-LCPU-6 samples had an intrinsic viscosity of 0.400 dL/g at 30.0 °C, corresponding to the low molecular weight sample described in the previous paper of the series.[1]

Characterization Techniques. Thin films of 2,6-LCPU-6 were prepared by casting a 2% (w/v) solution of the polymer in 1,1,1,3,3,3-hexafluoro-2-propanol (99.8+%, Aldrich) onto disposable aluminum pans (for DSC and WAXS), glass slides (for optical microscopy), and potassium bromide windows (for IR), at room temperature. Following the fast evaporation of most of the solvent, in a laminar flow hood, the samples were vacuum dried at 60 °C overnight to remove residual HFIP. The complete removal of solvent was confirmed by the absence of the specific IR bands of HFIP.

Differential scanning calorimetric measurements were conducted with a Perkin-Elmer DSC-7, employing a 20 mL/min flow of dry nitrogen as a purge gas for the sample and reference cells. The coolant was an ice–water bath. The temperature and power ordinates of the DSC were calibrated with respect to the known melting point and heat of fusion of a high-purity indium standard.

Room-temperature *X-ray diffraction* (XRD) patterns were recorded on flat films with a Statton X-ray camera using Ni-filtered Cu Kα radiation. The sample was contained in 1.5-mm Lindemann glass tubes and was mounted directly on the pinhole with the help of double stick tape. The X-ray camera length was calibrated with the 2.319-Å diffraction line of NaF and 3.035-Å diffraction line of $CaCO_3$. The X-ray films were measured for interplanar spacing data with a Supper circular film measuring device. Furthermore, from the powder pattern films, the radial XRD profiles were obtained with the use of an Optronics C-4500 2D microdensitometer and the Polygraf X-ray diffraction software.[29]

Optical microscopy was performed on a Carl-Zeiss Ultraphoto II polarizing microscope equipped with a Linkham Scientific Instruments TMS 90 temperature controller and a TMH 600 hot stage. The hot-stage temperature was calibrated with vanillin and potassium nitrate melting point standards.

Infrared spectroscopic data were obtained using an IBM Model 32 Fourier transform infrared spectrometer. Spectra were collected at 2-cm^{-1} resolution A minimum of 40 scans was signal averaged, and the spectrum was stored on magnetic storage media. The films used in this study were sufficiently thin to be within an absorbance range where the Beer–Lambert law is obeyed. Elevated temperature spectra were obtained by placing thin films between potassium bromide windows, in a temperature-controlled cell. The temperature was monitored via a thermocouple placed adjacent to the KBr windows and was controlled within 1 °C. The heating rate was 20 °C/min from room temperature to 90 °C and 5 °C/min from 90 to 220 °C. Before each spectral acquisition the temperature was kept constant for 10 min to ensure complete temperature equilibration along the sample cell. At the end of the first heating scan (up to 220 °C), the sample was cooled slowly to room temperature, followed by a second, third, and fourth heating scan in a similar fashion.

Results and Discussion

As has been reported in the first paper of this series, the 2,6-LCPU-6 requires cooling rates much faster than 100 °C/min in order to avoid homogeneous nucleation and crystallization and to bring the sample into the mesophase. It is easily understood that this kind of behavior makes difficult the preparation of thin films with mesophase morphology appropriate for spectroscopic analysis. The need for a quick and versatile way of producing such films led to a study of the casting behavior of 2,6-LCPU-6 from a variety of solvents, such as dioxane, THF, DMSO, DMAC, DMF, and HFIP. The solubility of 2,6-LCPU-6 in the above solvents increases in the order listed, and for the low boiling point ethers such as dioxane and THF, elevated temperatures need to be employed. Casting a 2% (w/v) solution of the polymer in the above solvents (except HFIP), at room temperature, resulted mainly in films with crystalline morphology (DSC and WAXS analyses were used to characterize the sample morphology) due to crystallization prior to solvent removal. On the other hand, the great solubility power of HFIP,[1,30] along with its low boiling point (bp = 59 °C), produced a thin film with the desired mesophase morphology. Before we proceed with the vibrational analysis of these thin films, it is essential to understand their structure and morphology in more detail.

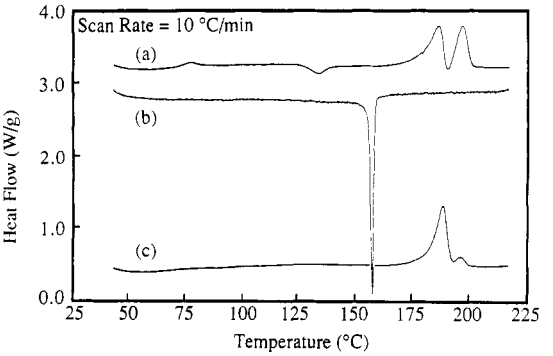

Figure 1. 10 °C/min DSC traces of HFIP-cast, 2,6-LCPU-6 thin film: (a) first heating scan; (b) first cooling scan; (c) second heating scan.

Differential Scanning Calorimetry. Typical 10 °C/min heating and cooling traces of 2,6-LCPU-6 thin films cast from HFIP are illustrated in Figure 1. Upon the first heating scan (a), the familiar step in heat capacity, corresponding to the glass transition (T_g), is observed at approximately 72 °C, along with a small enthalpy relaxation[4,31] endotherm peaking at 76 °C. This rather distinct glass transition behavior compared to the broad step in heat capacity generally obtained from melted samples (Figure 4) was the first indication of the amount of disorder present in the cast films due to the rapid solvent evaporation. The exotherm peaking at 133 °C (ΔH = 6.6 J/g; $\Delta S = 1.6 \times 10^{-2}$ J/g·K) is the most important feature in this DSC heating scan. In the first paper of this series[1] the nature of this exotherm was discussed extensively and it has been attributed to the mesophase–crystal transition. Cheng et al.[14] observed similar behavior with a thermotropic polyether, and they characterized it accordingly as arising from the monotropic nature of the liquid crystal. This exothermic transition upon heating is the characteristic signature of the monotropic liquid crystalline state. It arises primarily from the greater thermodynamic stability of the crystalline phase versus the mesophase, which defines the thermodynamic potential for this transition. A schematic plot of the temperature dependence of the Gibbs free energy (Figure 2) is a convenient way to express the relative thermodynamic stability of the crystalline, liquid crystalline, and liquid phases. The solid lines in Figure 2 represent the equilibrium temperature dependences of each phase. (Note that each sample can be a composite of many individual phases.) Additionally, kinetic factors such as sample mobility (which is a function of chain flexibility, mesophase structure, molecular weight, impurities, etc.) and chemical repeat regularity influence the overall process. According to

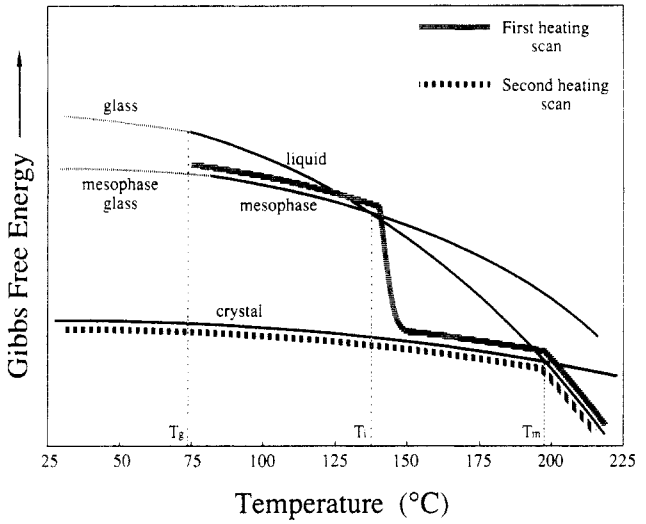

Figure 2. Schematic temperature dependence of Gibbs free energy for 2,6-LCPU-6 (see text for details).

Figure 2 (first heating scan), the mesophase–crystal transition must be located immediately above the mesophase–liquid "intersection", due to the limited mobility of the highly ordered (higher than smectic C) mesophase.

Following the 133 °C exotherm in Figure 1a, we observe two endotherms with maxima at 186 and 197 °C. The overall ΔH_m from 116 to 204 °C is 40.1 J/g. These two peaks have been assigned[1] to the crystalline melting transitions of two macroscopically distinct morphologies—a spherulitic morphology produced from slow cooling and a threaded crystalline morphology produced upon heating from the quenched mesophase. Similar behavior has been observed for the 2,4-LCPU-6, as well as other monotropic liquid crystalline polymers.[14] Upon cooling, a sharp exotherm around 157 °C followed by a 25 °C exothermic "tail" is observed. The overall ΔH_c from 121 to 165 °C is 40.6 J/g. This exotherm was reported in the previous paper of the series and attributed to a combined mesophase–crystallization process. The slow cooling rate (10 °C/min) of the first cooling scan resulted in a crystalline sample, as proven by the absence of the 133 °C exotherm in Figure 1c. Therefore, the second heating scan is expected to follow a different route on the temperature-dependent Gibbs free energy diagram of Figure 2, indicated by the thick broken curve, showing only a crystal melting transition. This in fact occurs, with the two familiar melting endotherms at 188 and 197 °C. The overall ΔH_m from 133 to 202 °C is 40.3 J/g, almost identical with its counterpart from Figure 1a (40.1 J/g).

X-ray Diffraction and Optical Microscopy. Figure 3 illustrates the radical *X-ray diffraction* (XRD) profiles of these thin films as a function of thermal history. The temperatures noted on Figure 3 represent the maximum temperatures to which these films were exposed during a 10 °C/min heating scan, followed by a quick quench to room temperature. The room temperature (35 °C) radial XRD profile verifies the low degree of order of these films upon casting, previously inferred from the DSC T_g behavior. The poorly resolved 002, 004, and 008 smectic layer reflections at 27.$_3$ Å ($2\theta = 3.2_4°$), 13.7 Å ($2\theta = 6.45°$), and 6.8 Å ($2\theta = 13°$), respectively, correspond to a 54.$_9$-Å repeat, much shorter than the 57.$_6$ Å of the melt-quenched sample.[1] The broad and diffuse wide-angle reflection with a maximum at 4.5 Å ($2\theta = 19.8°$) is a product of the convolution of the 4.5 Å ($2\theta = 19.8°$), 4.0 Å ($2\theta = 22°$), and 3.3 Å ($2\theta = 27°$) reflections. The strongest 4.5-Å reflection arises from lateral stacking of the biphenyls, while the

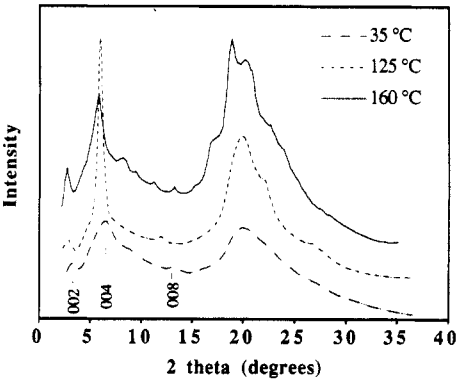

Figure 3. Room-temperature radial *X-ray diffraction* (XRD) profiles of HFIP-cast, 2,6-LCPU-6 thin films as a function of thermal history. The noted temperature corresponds to the maximum temperature to which these films were exposed during a 10 °C/min heating scan, followed by a quick quench to room temperature.

other two wide-angle reflections arise from the dimensional correlation of the TDI moieties.[1] Evidently the rapid solvent evaporation results in a less ordered smectic structure with a repeat distance almost 3 Å shorter than the "equilibrium", higher than smectic C, mesophase structure. Further proof of the mesophasic character of these thin films comes from the *schlieren* textures observed under the polarizing optical microscope. These schlieren textures are similar to those published elsewhere.[1]

Upon temperature increase this poorly ordered smectic structure transforms slowly into a more highly ordered one, as shown by the (125 °C) radial XRD profile of Figure 3. The highly resolved 002, 004, and 008 smectic layer reflections correspond to a 58.$_1$-Å repeat, almost identical to the 58.$_2$-Å repeat from the melt-quenched sample heated at 125 °C.[1] The strong correlation of the smectic layers imposes a better lateral stacking of the chains which results in stronger and sharper wide-angle reflections (4.5, 4.0, and 3.3 Å). Upon further temperature increase the mesophase to crystal transition takes place, clearly indicated by the (160 °C) radial XRD profile of Figure 3. The 002 and 004 reflections of the (160 °C) curve correspond to a 58.$_5$-Å repeat which is in complete agreement with the bulk 2,6-LCPU-6 crystal structure.

A careful observation of the two crystal melting endotherms of Figure 1a shows that they are separated by a small exotherm, indicative of a melting-recrystallization[32] process. This process occurs faster in the solvent-cast films than in the samples quenched from the melt. However, samples previously annealed at 165 °C show little melting-recrystallization between the higher and the lower peak.[1] Apparently, the method of sample preparation controls the degree of chain entanglement as well as the free volume, affecting drastically the behavior of this strongly intermolecularly interacting system. Further demonstration of the effect of sample preparation upon the underlying transitions is presented in Figure 4. A rapid examination of the four scans (Figures 4a–c and 1a) indicates that all of them look very much alike, except that of Figure 4c which possesses an additional endotherm at 113 °C, 20 °C below the mesophase–crystal transition. As a result of MeOH Soxhlet extraction the sample of Figure 4c has been shown[1] to exhibit a perfected mesophase structure and macroscopic morphology. In addition, the enthalpy associated with the 113 °C endotherm is almost the same as that of the 133 °C exotherm (Table I). This sort of behavior suggests a mesophase melting prior to crystallization. For the rest of the quenched samples, mesophase imperfections result in melting over a broad tem-

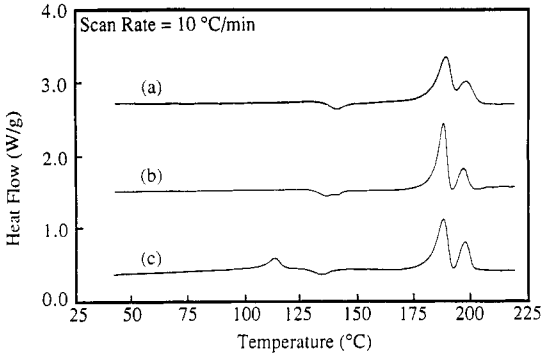

Figure 4. 10 °C/min DSC heating traces of 2,6-LCPU-6: (a) sample quenched into liquid N_2 from the melt; (b) fiber drawn from the melt; (c) fiber drawn from the melt, Soxhlet-extracted in hot MeOH for 4 days, and vacuum dried at 60 °C overnight. (See Table I for transition temperatures and enthalpies.)

perature range and make this transition diffuse and difficult to observe. The fact that this peak occurs 30–40 °C higher than the T_g rules out the possibility that it is an enthalpy relaxation peak from a more ordered[4] "mesophase glass".

Table I lists the transition temperatures and enthalpies observed for the four different techniques of freezing the sample into the mesophase (Figures 4 and 1a). Moving from left to right, the mesophase–crystal transition temperatures show an apparent trend toward lower temperatures. The same trend, only much weaker, can be noted for the threaded morphology crystal melting temperatures, indicating that these crystals developed from the mesophase. In contrast to the above, the spherulitic morphology crystal melting temperature remains constant at 197 °C. The explanation of these phenomena lies in the method of sample preparation. Solvent treatment results in greater sample free volume and fewer chain entanglements, which yields greater mobility and lower transitions. On the other hand, the spherulitic morphology crystalline regions preexisted before the mesophase to crystal transition, making their melting temperatures insensitive to sample preparation.

Infrared Spectroscopy. The room-temperature infrared spectrum of a HFIP-case, 2,6-LCPU-6 thin film is illustrated in Figure 5. A total of 19 out of the 31 observable peaks and peak shoulders have been assigned (Table II) from spectral comparisons of 2,6-LCPU-6, similar polymers, and model compounds in the literature,[5,17,18,26,28] as well as of our own. Specifically the mesogenic polyurethanes 2,4-LCPU-6[26-28,33] and 1,3-LCPU-6,[34] which are polycondensation products of BHHBP with 2,4-TDI and 1,3-PDI (1,3-PDI stands for the meta-substituted 1,3-phenyl diisocyanate), respectively, aid in the vibrational peak assignments of the meta-substituted phenyl ring (TDI moiety). On the other hand, normal polyurethanes like the 2,6-PU-6, 2,4-PU-6, and 1,3-PU-6, which are polycondensation products of hexanediol with 2,6-TDI, 2,4-TDI, and 1,3-PDI, respectively, aid in the peak assignments of the biphenol moiety. Last but not least, the low molecular weight diurethanes from the reactions of 2,6-TDI, 2,4-TDI, and 1,3-PDI with MeOH assist in the hexamethylene moiety peak assignments.

There are distinct differences between the spectra measured at room temperature and those at high temperatures, mainly due to peak shifts (Table II) and intensity changes. Major differences can be identified between 3200–3500 cm^{-1} (NH stretch region), 1690–1735 cm^{-1} (carbonyl stretch, amide I region), 1500–1550 cm^{-1} (amide II region), 1590–1600 cm^{-1} (TDI benzene ring C=C stretch region), 1600–1620 cm^{-1} (biphenyl C=C stretch region), and 810–830 cm^{-1} (biphenyl out-of-plane CH wag region). The changes occurring in these regions in intensities, peak sharpness, and peak shifts will be discussed in detail in order to understand the 2,6-LCPU-6 phase behavior better.

Figure 6 displays the amide I region recorded as a function of increasing temperature for the first and the second heating scan of a freshly cast thin film of 2,6-LCPU-6 on a KBr window. The spectra in Figure 6 have not been arbitrarily scaled and are shown on an equal absorbance scale. It is well-known that the infrared absorbance of H-bonded urethane carbonyl appears at lower wavenumbers than that of free urethane carbonyl.[23,35,36] The amide I infrared spectra of semicrystalline samples such as nylons[37,38] and polyurethanes[26,39] have been reported to comprise distinct spectral features due to the degree of carbonyl H-bonding. It has been proposed that there are three overlapping peaks in the amide I region.[37] In order of increasing wavenumbers, these are H-bonded carbonyl groups in ordered ("crystalline") domains, H-bonded carbonyl groups in disordered ("amorphous") conformations, and non-H-bonded (free) carbonyl groups. Accordingly, the well-resolved peak in the vicinity of 1699 cm^{-1} in Figure 6 is assigned to the ordered hydrogen-bonded (crystalline) carbonyl stretch. Possible multiple peaks similar to those observed from the asymmetrically substituted 2,4-LCPU-6[28,39] are less likely to occur in 2,6-LCPU-6 due to the single type of urethane linkage (ortho to the methyl group of the TDI moiety) versus the dual type (ortho and para) in 2,4-LCPU-6.

It is apparent from Figure 6 that two distinct transitions occur in the spectral shape. The spectra for the first heating scan (Figure 6A) have been separated to facilitate visualization of a transition that involves the sudden appearance of the well-defined ordered H-bonded carbonyl stretch above 120 °C. The second transition (isotropization) is easily observable in both first and second heating scans (figure 6A,B) as an abrupt decrease in H-bonding at the melting point (above 180 °C). The fact that the third and fourth scans are identical to the second one excludes any possibility of sample decomposition. The freshly cast film has a mesophase structure as shown on the basis of DSC and X-ray scattering. The cooling rate in the IR experiments was less than 10 °C/min, so that any subsequent scans after the first one involve a crystalline sample.

To make these features clearer, we plotted the peak absorbance of each band as a function of temperature. There are a variety of methods to extract the peak absorbance from an IR spectrum. Some of them, such as the pseudo-base-line method, the subtraction method, and the curve-fitting method have been applied[18] to the present system. However, the pseudo-base-line method was used mainly, accompanied with curve fitting which will be discussed later.

Figure 7 illustrates the peak absorbance of the first and second heating scans as a function of temperature for the 1699-cm^{-1} ordered H-bonded carbonyl band (A) and the 2941-cm^{-1} CH_2 out-of-phase stretching band (B). The CH_2 out-of-phase stretching band has been used in the past as an internal standard for infrared thermal analysis of polyurethanes.[25,40] With that in mind, Figure 7B was included to prove that the changes in the peak absorbance of the ordered H-bonded carbonyl groups reflect intermolecular changes, rather than changes arising from sample thickness. In addition, there is no significant difference observed between the first and second heating scan. Furthermore, Figure 7B demonstrates the lack of sensi-

Table I
DSC Transition Temperatures and Enthalpies from Figures 4 and 1a (10 °C/min Heating Scans)

transn element	melt, quenched in liquid N_2 (Figure 4a)	fiber drawn from the melt (Figure 4b)	fiber, Soxhlet-extracted in hot MeOH (Figure 4c)	thin film, cast from HFIP (Figure 1a)
mesophase melting temp[a] (°C)			113	
mesophase–cryst transn temp (°C)	140	136/141	$133._1$	$133._0$
threaded morph cryst melting temp (°C)	$189._0$	$188._2$	$187._8$	$186._4$
spherulitic morph cryst melting temp (°C)	197	197	197	197
mesophase melting enthalpy[a] (J/g)			7.0	
mesophase–cryst transn enthalpy (J/g)	−5.8	−4.2	−6.6	−6.6
overall cryst melting enthalpy (J/g)	47.2	39.4	40.8	46.7

[a] See text for details.

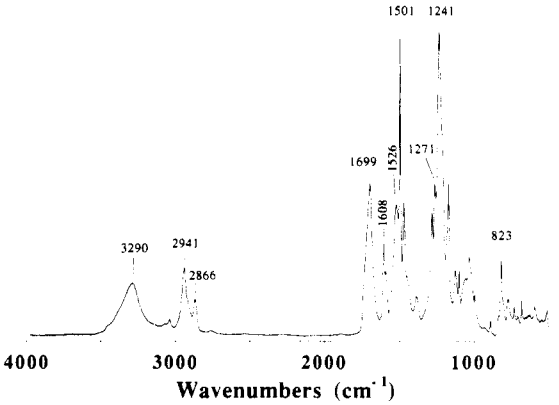

Figure 5. Survey FTIR spectrum of a HFIP-cast, 2,6-LCPU-6 thin film, taken at room temperature.

Table II
Infrared Band Assignments for 2,6-LCPU-6

peak frequency (cm^{-1}) at 25 °C	peak frequency (cm^{-1}) at 200 °C	assignment
3430[a]	3430[a]	free NH stretch
3290	3307	H-bonded NH stretch
3039	3034	aromatic CH stretch
2941	2940	CH_2 stretch (out-of-phase stretch)
2866	2865	CH_2 stretch (in-phase stretch)
1734[a,b]	1740[a,b]	"free" amide I mode ("free" C=O stretch)
1702[a,b]	1720[a,b]	disordered H-bonded amide I mode
1697[a,b]	1696[a,b]	ordered H-bonded amide I mode
1608	1604	benzene ring C=C stretch (biphenyl > TDI)[c]
1594	1593	benzene ring C=C stretch (TDI)
1526	1521	amide II
1501	1498	benzene ring semicircle stretch
1464	1464[a]	CH_2 deformation
1271	1266	aromatic ether CO[d]
1241	1237	aromatic ether CO[d]
823	821	out-of-plane CH wag of biphenyl
713	709	out-of-plane NH wag
652	652	out-of-plane C=O wag
518	522	out-of-plane quadrant benezene ring bend (biphenyl)

[a] Estimated from peak deconvolution. [b] The present value corresponds to the second heating scan (see text for details). [c] The biphenyl moiety contributes mostly to the absorbance of this peak, with a smaller contribution from the TDI moiety as well. [d] The present assignment bears a small degree of uncertainty because of a great deal of peak overlapping in this spectral region.

tivity of the CH_2 out-of-phase stretching vibration to the phase transitions occurring within the temperature range of interest. The same is not true for the first and second heating scans of Figure 7A. Apart from the melting transition above 180–200 °C, accompanied by a drastic decrease in the ordered H-bonded amide I absorbance in both scans, there is another transition around 130 °C in the first heating scan only. This corresponds to the mesophase–crystal transition, which is accompanied by a dramatic increase in the ordered H-bonded peak intensity during crystallization between 120 and 140 °C. This is in agreement with our previous findings[4] where it was established through H-bonding elimination that the mesophase arises primarily from the biphenol alignment, and the presence or absence of H-bonding is not important. Although this transition has been observed previously from DSC and X-ray diffraction, IR spectroscopy provides a technique to probe the localized microstructural changes taking place during this phase transition. In order to analyze the data quantitatively, it is necessary to resolve the amide I mode into its constituents.

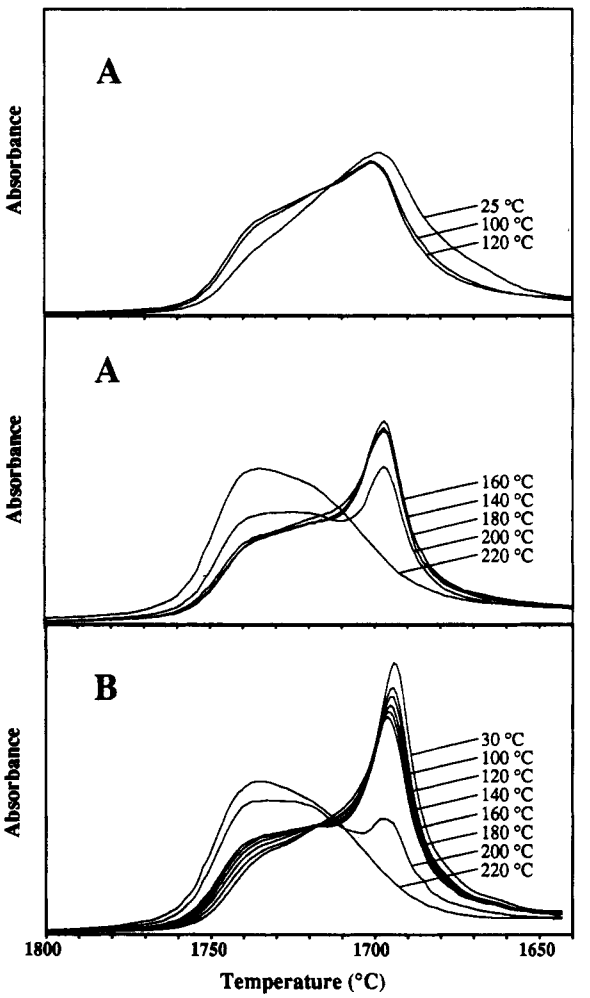

Figure 6. FTIR spectra of the amide I region (1640–1800 cm^{-1}) of a HFIP-cast, 2,6-LCPU-6 thin film as a function of increasing temperature: (A) spectra recorded on the first heating scan; (B) spectra recorded on the second heating scan.

As has been pointed out extensively,[37,38,41,42] deconvolution of overlapping peaks leading to a unique solution is generally not possible. Without previous knowledge of

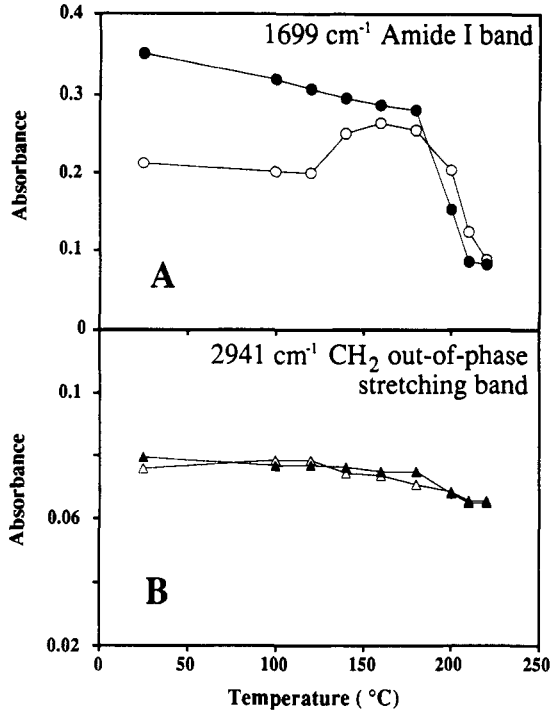

Figure 7. Peak absorbance as a function of temperature for the 1699-cm^{-1} ordered H-bonded amide I band (A) and the 2941-cm^{-1} CH_2 out-of-phase stretching band (B). First heating scan data are indicated with unfilled symbols and second heating scan data with filled symbols.

the band shape, the number, position and breadth of the bands, base-line position, etc., one can arrive at almost any desired solution. Even with a knowledge of the number of bands, good prior estimates of the above-mentioned factors are necessary prerequisites for obtaining valid solutions. For this reason we followed step by step the well-established amide I deconvolution technique of Painter and Coleman.[37,38,42] In particular, the essential starting parameters were extracted from the analysis of semicrystalline nylon 11 of Skrovanek et al.[37]

In summary, each spectrum recorded at different temperatures was resolved into three components (two above the crystalline melting point), using the following procedure.

(1) The band shape of all three peaks was assumed to be Gaussian. Curve-fitting attempts allowing band shape to vary proved to favor the pure Gaussian band shape by a least-squares criterion. Imposing Lorentzian band shape on the ordered H-bonded amide I peak changes substantially the relative values of the deconvoluted peak area but does not change the temperature dependence.

(2) A linear base line was assumed from 1800 to 1630 cm^{-1} and minimized as well, during curve fitting. Although the "correct" base line is rather subjective, the base-line choice again affects mostly the absolute values of the deconvoluted peak area but does not change the temperature dependence.

(3) Curve fitting was limited to the spectral data of the amide I region between 1800 cm^{-1} (left end) and 1630–1643 cm^{-1} (right end). The low-wavenumber end was determined as the minimum between the 1699- and 1608-cm^{-1} peak. Although the two peaks are well separated and the low-wavenumber end lies on a fairly shallow minimum, one can anticipate a certain degree of interference from the wing of the 1608-cm^{-1} peak with the base line. This deviation is just about visible at the right wing of each spectrum of Figure 8. This does not lead to significant error but is certainly the weakest point of the curve-fitting procedure.

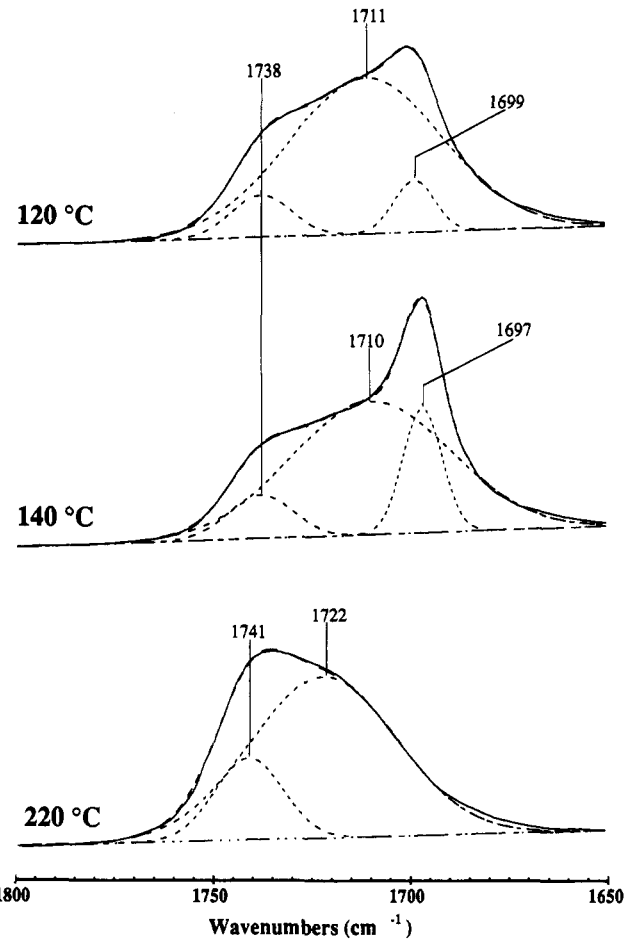

Figure 8. Least-squares deconvolution of the amide I region of a HFIP-cast, 2,6-LCPU-6 thin film from the first heating scan at 120, 140, and 220 °C.

Figure 8 presents the least-squares fitting results of the amide I region of a HFIP-cast, 2,6-LCPU-6 thin film from the first heating scan at 120, 140, and 220 °C. Each spectrum is representative of the series of spectra in between the two phase transitions mentioned above. The main component of the 120 °C spectra is the disordered H-bonded amide I band. This is consistent with the DSC and X-ray diffraction data showing that the sample exhibits smectic mesophase morphology. The higher than smectic C mesophase of 2,6-LCPU-6 reported elsewhere[1] has the required chain conformation to place both carbonyls of the TDI moiety in close proximity with the NH groups of the neighboring TDI moiety. The variation in distance and angle between the neighboring NH and C=O groups generates the large width at half-height ($W_{1/2,d}$) (55–60 cm^{-1}) of the disordered H-bonded amide I peak with respect to the 18–25 cm^{-1} and 14–15 cm^{-1} for the "free" and ordered H-bonded amide I peaks. Above the mesophase to crystal transition (140 °C) the ordered H-bonded amide I peak increases by more than a factor of 2 compared to the disordered one, as would be expected for this transition. Upon further heating, sample isotropization occurs, manifested by the disappearance of the ordered H-bonded amide I peak in the 220 °C spectrum.

The detailed results of the curve fitting of the amide I region throughout the temperature range 25–220 °C are given in Tables III and IV for the first and second heating scans, respectively. The curve-fitting data summarized in Tables III and IV are plotted in Figures 9–11 to facilitate better visualization of the underlying transitions. The changes in the areas of the ordered (A_o) and disordered (A_d) H-bonded amide I peaks (Figure 9) show unequiv-

Table III
Deconvolution Results for the Amide I Region of a HFIP-Cast 2,6-LCPU-6 Thin Film[a] (First Heating Scan)

	hydrogen bonded											
	ordered			disordered			"free"					
temp, °C	ν, cm^{-1}	$W_{1/2}$, cm^{-1}	A_o	ν, cm^{-1}	$W_{1/2}$, cm^{-1}	A_d	ν, cm^{-1}	$W_{1/2}$, cm^{-1}	A_f	A_t	A_o/A_t	A_d/A_t
25	1697.3	15.6	0.520	1704.5	61.6	9.22	1736.2	17.6	0.289	10.0	0.0519	0.919
100	1698.7	14.7	0.597	1709.7	56.8	8.06	1737.0	21.3	0.739	9.40	0.0635	0.858
120	1698.8	14.6	0.681	1711.2	55.9	7.70	1737.6	21.6	0.806	9.18	0.0742	0.838
140	1696.9	13.9	1.52	1709.9	56.8	6.65	1738.0	23.1	0.868	9.04	0.169	0.735
160	1697.0	13.8	1.72	1710.2	59.2	6.60	1738.5	23.0	0.823	9.15	0.188	0.722
180	1697.3	13.6	1.65	1711.0	59.5	6.49	1738.9	23.0	0.940	9.08	0.182	0.714
200	1696.1	14.1	1.71	1719.8	52.0	6.15	1740.2	24.6	1.12	8.99	0.191	0.685
220				1721.6	51.5	7.20	1740.8	25.2	1.88	9.08		0.793

[a] A_o = area (arbitrary units) of band attributed to ordered domains, A_d = area (arbitrary units) of band attributed to mesophase and amorphous domains, A_f = area (arbitrary units) attributed to "free" carbonyl groups, and A_t = total area = $A_o + A_d + A_f$. $W_{1/2}$ = width at half-height of Gaussian curve.

Table IV
Deconvolution Results for the Amide I Region of a HFIP-Cast 2,6-LCPU-6 Thin Film[a] (Second Heating Scan)

	hydrogen bonded											
	ordered			disordered			"free"					
temp, °C	ν, cm^{-1}	$W_{1/2}$, cm^{-1}	A_o	ν, cm^{-1}	$W_{1/2}$, cm^{-1}	A_d	ν, cm^{-1}	$W_{1/2}$, cm^{-1}	A_f	A_t	A_o/A_t	A_d/A_t
30	1693.7	11.8	1.90	1702.0	50.4	7.09	1734.4	26.3	1.33	10.3	0.185	0.687
100	1694.3	12.4	1.84	1704.0	52.0	6.75	1735.8	26.9	1.39	9.98	0.184	0.677
120	1694.5	12.7	1.84	1705.4	54.1	6.73	1736.6	26.9	1.41	9.98	0.184	0.675
140	1694.8	12.9	1.83	1706.7	56.0	6.68	1737.2	26.9	1.44	9.94	0.184	0.671
160	1695.2	13.3	1.84	1707.7	57.3	6.58	1737.7	27.1	1.47	9.89	0.186	0.665
180	1695.5	13.5	1.83	1708.6	59.2	6.63	1738.2	27.2	1.45	9.91	0.184	0.669
200	1695.9	13.9	0.889	1719.8	52.1	6.78	1740.2	26.0	1.65	9.32	0.0954	0.727
220				1721.6	51.7	7.09	1740.8	25.7	1.89	8.98		0.790

[a] A_o = area (arbitrary units) of band attributed to ordered domains, A_d = area (arbitrary units) of band attributed to mesophase and amorphous domains, A_f = area (arbitrary units) attributed to "free" carbonyl groups, and A_t = total area = $A_o + A_d + A_f$. $W_{1/2}$ = width at half-height of Gaussian curve.

ocally that the 130 °C transition is associated with the mesophase to crystal transition. It is characteristic that the entire fraction of carbonyl groups which transform to the crystal (ordered) phase originates from the mesophase (disordered H-bonded carbonyl groups), while the "free" carbonyl content shows a monotonic increase. The same transition is also visible from the peak position and width at half-height of the ordered and disordered H-bonded amide I peaks in Figures 10 and 11, respectively. The 130 °C transition is reflected by a sudden decrease in the peak frequencies of both H-bonded carbonyl groups (Figure 10). This is indicative of a substantial lateral ordering taking place in both phases. On the other hand, while the width at half-height of the ordered H-bonded amide I peak continues to shift to lower values as anticipated, the disordered one shows a different behavior. Below 130 °C this peak arises from the mesophase which perfects itself and narrows its width at half-height. Above 130 °C the nature of this peak changes. An assembly of imperfect crystalline domains (portion of the mesophase which did not manage to achieve crystalline order) along with the remaining amorphous fraction contributes to the width increase observed.

Although the main goal of the curve-fitting analysis was to analyze the mesophase to crystal transition, it also proved useful in the analysis of the melting transitions. In the DSC section of this paper we observed the melting behavior of crystalline regions with different macroscopic morphologies. The first heating scan resulted (through a melting-recrystallization process) in the higher melting point spherulitic rich sample (Figure 1a). On the other hand, the slow cooling rate of the first cooling scan resulted in a threaded texture rich sample which melts at a lower temperature (Figure 1c). Figure 9 reflects these features. Characteristically, the lower value of the A_o at 180 °C versus the 160 and 200 °C values reinforces the evidence for a melting-recrystallization process taking place during the first heating scan. Figures 10 and 11 indicate substantial changes in the disordered H-bonded carbonyl portion above 180 °C. It is worth noting that these changes occur prior to the melting of the crystalline domains (188 and 197 °C from DSC). This suggests that above 180 °C imperfect crystalline domains cannot exist. Therefore, the disordered H-bonded amide I peak changes in this temperature region are identified with a molten, quite mobile H-bonded carbonyl group shifting its frequency 10 cm^{-1} higher and its width at half-height 7 cm^{-1} lower. On the other hand, the changes in the "free" amide I peak are much smaller upon melting and mostly occur also above 180 °C.

As pointed out previously,[37,42] unlike the NH stretching region, the total area of the amide I region (A_t) does not vary appreciably with temperature, and the absorptivity coefficients can be assumed the same for the three different bands. Skrovanek et al.[37] in their study of nylon 6 reported the total area of the amide I region to vary approximately 7%. Tables III and IV as well as Figure 9 indicate a 5 and 7% variation for the first and second heating scans, respectively. The values of A_t for the first heating scan were found to be 5–6% lower than those for the second heating scan. We believe that this arises primarily from the quick solvent evaporation that produces a slightly opaque thin film which contributes to scattering. The same values of A_t above the melting point provide adequate proof of the validity of the above argument. Figure 10 indicates that all three peaks of the first scan exhibit peak positions (ν) at higher wavenumbers than those of the second scan, below the melting point. This is a clear manifestation of the effect of fast solvent evaporation on the average hydrogen bonding that affects the strength of

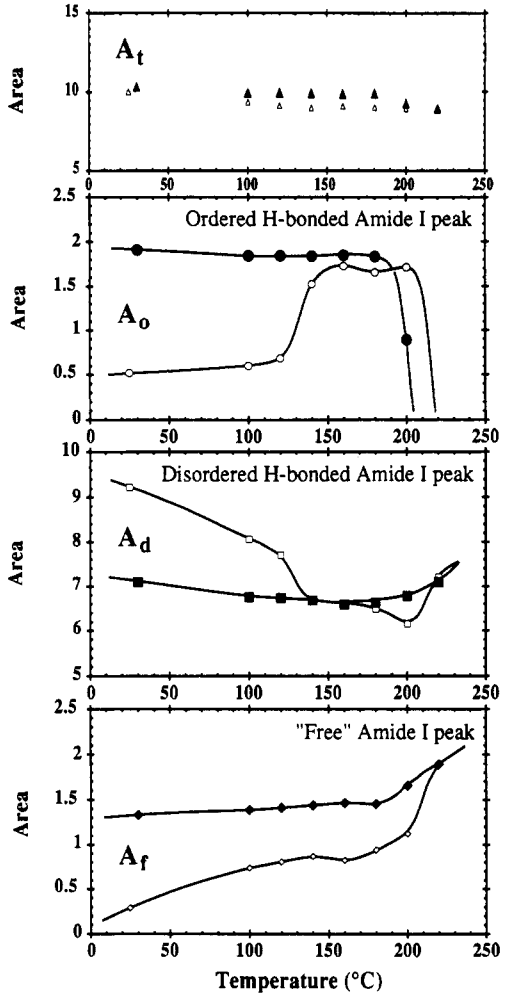

Figure 9. Plots of the areas of the "free" (A_f), disordered (A_d), and ordered (A_o) H-bonded peaks as well as the total (A_t) carbonyl groups obtained from the amide I region as a function of temperature. First heating scan data are indicated with unfilled symbols and second heating scan data with filled symbols.

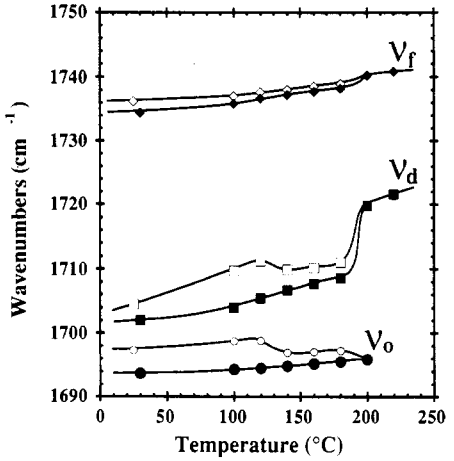

Figure 10. Plots of the peak frequency of the "free" (ν_f), disordered (ν_d), and ordered (ν_o) H-bonded carbonyl peaks from the amide I region as a function of temperature. First heating scan data are indicated with unfilled symbols and second heating scan data with filled symbols.

the intermolecular interactions as well as the sample free volume.

A measure of the inaccuracy of our curve-fitting analysis is indicated from the ν_f curves of Figure 10. Theoretically the two lines should coincide. By taking the average of the two ν_f and not allowing the computer to vary it, we derive less than 1% error in the area values of A_f and A_d

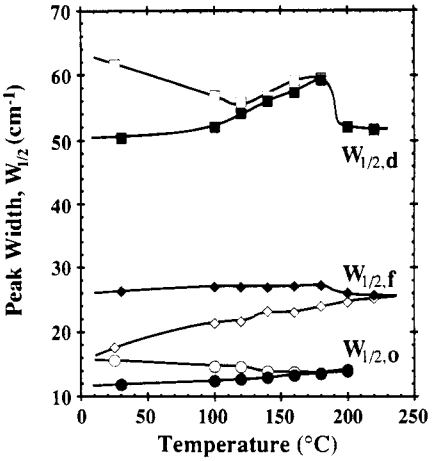

Figure 11. Plots of the width at half-height of the "free" ($W_{1/2,f}$), disordered ($W_{1/2,d}$), and ordered ($W_{1/2,o}$) H-bonded carbonyl peaks from the amide I region as a function of temperature. First heating scan data are indicated with unfilled symbols and second heating scan data with filled symbols.

and much less for the A_o. In the same study of nylon 11, referenced above, Skrovanek et al. reported that the fraction of ordered H-bonded amide groups in nylon 11 provides a good estimate of the sample crystallinity. On the basis of a similar argument, we can estimate our sample crystallinity to be between 18 and 19% (Tables III and IV).

In the NH stretching region (3500–3200 cm^{-1}) of 2,6-LCPU-6 the peak observed at 3290 cm^{-1} is assigned to the ordered H-bonded NH stretch,[36,43] while the shoulder at 3430 cm^{-1} is typically assigned to the "free" NH stretch. Infrared spectroscopic data of polyamides and polyurethanes in the NH stretching region have been used in the past to calculate some thermodynamic parameters.[44,45] However, Coleman et al.[23,37,42,46] pointed out the strong dependence of the extinction coefficient upon frequency, which is highly affected by the H-bond strength. Unlike the amide I vibration which is sensitive to conformation through dipole–dipole interactions, the NH stretching mode is more or less conformationally insensitive. Therefore, we did not attempt to extract information similar to that obtainable from the amide I mode but systematically monitored the temperature dependence of the peak absorbance of the ordered H-bonded NH stretch (Figure 12A). Features similar to those observed in the carbonyl stretching region can be seen here. Molecular simulations of 2,6-LCPU-6[47] indicate complete H-bonding formation between the NH and C=O groups in the crystal lattice. Therefore, it is expected for the NH stretching region to behave similarly to that of the carbonyl. Figure 12B shows the peak absorbance of the amide II region (1526 cm^{-1}) as a function of temperature. Its features are almost identical to those of the H-bonded C=O and NH stretch mentioned previously.

Figures 7–12 described the changes in H-bonding during the mesophase–crystal transition. It is also of interest to monitor the behavior of the mesogenic moiety during this process. Figure 13A depicts the temperature dependence of the peak absorbances for two different vibrational modes of the biphenyl benzene ring. The peak at 823 cm^{-1} is assigned to the out-of-plane CH wag of the biphenyl, while the 1608-cm^{-1} peak is assigned to the biphenyl C=C stretch, and their peak absorbances are displayed on the upper and lower parts of Figure 13A, respectively. Although the exact influence of the intermolecular interactions on these vibration modes is not fully established, it is noteworthy to mention the following features. These

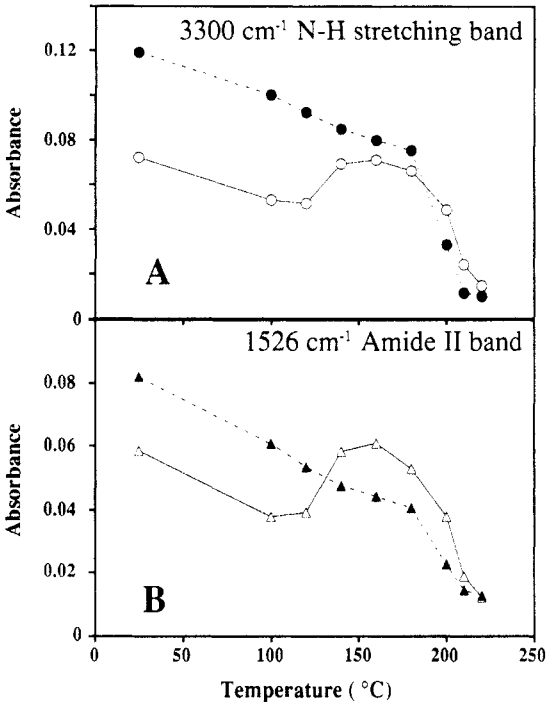

Figure 12. Peak absorbance as a function of temperature for the H-bonded NH stretching band (A) and the amide II band (1526 cm^{-1}) (B). First heating scan data are indicated with unfilled symbols and second heating scan data with filled symbols.

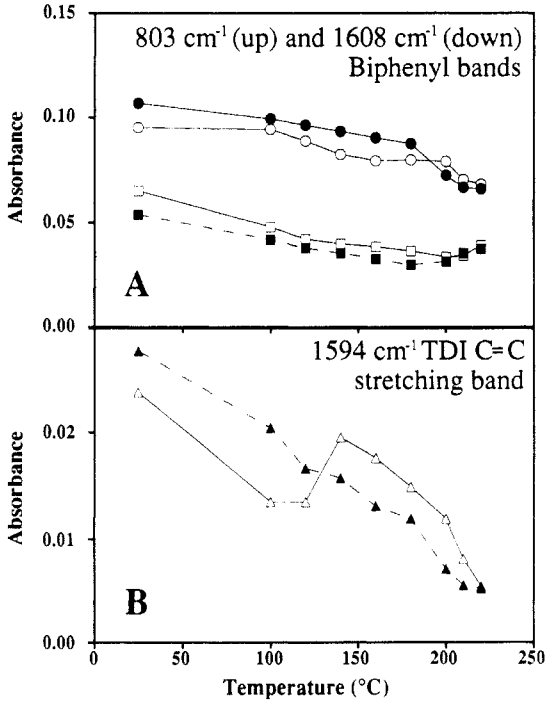

Figure 13. Peak absorbance as a function of temperature for the biphenyl out-of-plane CH wagging band (803 cm^{-1}) (upper pair of curves in A), the biphenyl C=C stretching band (1608 cm^{-1}) (lower pair of curves in A), and the TDI C=C stretching band (1594 cm^{-1}) (B). First heating scan data are indicated with unfilled symbols and second heating scan data with filled symbols.

peaks, associated with the biphenyl moiety, exhibit relatively small changes in the vicinity of the mesophase–crystal transition and somewhat greater changes at the melting transition (Figure 13A). In Figure 13B the temperature dependence of the 1594-cm^{-1} C=C stretch in the TDI moiety is displayed. This band exhibits behavior similar to that of the bands associated with H-bonding (Figures 7A and 12A,B). The direct bonding of the toluene ring (C=C stretch) to the urethane groups that undergo extensive H-bonding must be largely responsible for this result. An explanation can be proposed either on the basis of the presence of a coupled vibration mode between the benzene ring C=C stretch and the adjacent urethane groups, which undergo extensive H-bonding, or upon changes of the spatial arrangement of the bulky toluene ring during crystallization. Molecular simulations integrated with crystallographic analysis of 2,6-LCPU-6[47] reveal considerable changes in the spatial arrangement of the TDI rings upon crystallization in order to accommodate their bulky methyl group, but this argument alone is not sufficient to discriminate between the two alternative explanations.

Specific methylene bands, such as CH_2 rocking and CH_2 wagging, have been used extensively to analyze alkyl chain conformations from the infrared spectra of low and high molecular weight compounds.[15,16,19,20] The intense CH_2 rocking bands in the vicinity of 730 cm^{-1} from trans sequences, as well as some specific bands such as gtg′, gg, and gtt (end gauche) and (gtg and gtg′) in the 1300–1400-cm^{-1} region, have been heavily utilized for this purpose. Unfortunately, we were unable to assign these peaks definitively, because they were overlapped by other rather intense vibration peaks of 2,6-LCPU-6.

Conclusions

(1) DSC, WAXS, polarized optical microscopy, and infrared spectroscopy indicate that fast solvent evaporation from HFIP solutions results in 2,6-LCPU-6 thin films with a glassy mesophase morphology.

(2) The mesophase to crystal exothermic transition (monotropic liquid crystal) has been observed by DSC between 130 and 140 °C, depending on sample preparation. At 10–20 °C below this transition, the mesophase melting occurs, which provides adequate mobility for crystallization.

(3) Curve-fitting analysis of the conformationally sensitive amide I region resulted in a quantitative assessment of the temperature dependence of H-bonding. The behavior of the H-bonds correlated well with that expected from the results of calorimetric and WAXS studies.

(4) The mesophase to crystal transition has been observed by infrared spectroscopy to be between 120 and 140 °C, primarily on the basis of the substantial increase of the ordered H-bonded amide I peak and the decrease of the disordered H-bonded amide I peak in this temperature ramp. The crystal melting transition occurs between 180 and 210 °C and is accompanied by the complete disappearance of the ordered H-bonded amide I peak along with substantial changes in the frequency and width at half-height of the disordered H-bonded amide I peak.

Acknowledgment. We acknowledge valuable suggestions during the course of this study from Professors M. M. Coleman, P. C. Painter, K. Tashiro, and Mr. K. Ichikawa. We are grateful to the Center for UMass–Industry Research in Polymers (CUMIRP) and to the Army Research Office (Grant ARO-23941-CH) for financial support of this research. E.S. thanks Bridgestone Corp. for providing the opportunity for a sabbatical leave.

References and Notes

(1) Papadimitrakopoulos, F.; Hsu, S. L.; MacKnight, W. J., submitted to *Macromolecules*.
(2) Keller, A.; Ungar, G., to be published.
(3) Percec, V.; Keller, A. *Macromolecules* **1990**, *23*, 4347.
(4) (a) Papadimitrakopoulos, F.; Kantor, S. W.; MacKnight, W. J. *Recent Advances in Fiber and Polymer Science*; VCH Pub-

lishers: New York, to be published. (b) Papadimitrakopoulos, F.; Kantor, S. W.; MacKnight, W. J. *Polym. Prepr. (Am. Chem. Soc., Div. Polym. Chem.)* **1990**, *31* (1), 486.
(5) Smyth, G.; Pollack, S. K.; MacKnight, W. J.; Hsu, S. L. *Liq. Cryst.* **1990**, *7*, 839.
(6) Yang, X.; Waldman, D. A.; Hsu, S. L.; Nitzsche, S. A.; Thakur, R.; Collard, D. M.; Lillya, C. P.; Stidham, H. D. *J. Chem. Phys.* **1989**, *89*, 5950.
(7) Yang, X.; Kardan, M.; Hsu, S. L.; Collard, D.; Heath, R. B.; Lillya, C. P. *J. Chem. Phys.* **1988**, *92*, 196.
(8) Kardan, M.; Kaito, A.; Hsu, S. L.; Takur, R.; Lillya, C. P. *J. Phys. Chem.* **1987**, *91*, 1809.
(9) Kardan, M.; Reinhold, B. B.; Hsu, S. L.; Thakur, R.; Lillya, C. P. *Macromolecules* **1986**, *19*, 616.
(10) Lee, W. K.; Heiney, P. A.; McCauley, J. P., Jr.; Smith, A. B., III *Mol. Cryst. Liq. Cryst.* **1991**, *198*, 273.
(11) Gregoriou, V. G.; Chao, J. L.; Toriumi, H.; Palmer, R. A. *Chem. Phys. Lett.* **1991**, *179*, 491.
(12) Boeffel, C.; Spiess, H. W. *Macromolecules* **1988**, *21*, 1626.
(13) Goldfarb, D.; Luz, Z.; Zimmermann, H. *J. Chem. Phys.* **1983**, *78*, 7065.
(14) Cheng, S. Z. D.; Yandrasits, M. A.; Percec, V. *Polymer* **1991**, *32*, 1284.
(15) Tashiro, K.; Ono, K.; Minagawa, Y.; Kobayashi, M.; Kawai, T.; Yoshino, K. *J. Polym. Sci., Part B: Polym. Phys.* **1991**, *29*, 1223.
(16) Koenig, J. L. In *Advances in Polymer Science*; Meerwall, E. D. v., Frank, C. W., Semerak, S. N., Koenig, J. L., Eds.; Springer-Verlag: New York, 1984; Vol. 54; pp 87–154.
(17) Colthup, N. B.; Daly, L. H.; Wiberley, S. E. *Introduction to Infrared and Raman Spectroscopy*; Academic Press: New York, 1990.
(18) Bower, D. I.; Maddams, W. F. *The Vibration Spectroscopy of Polymers*; Cambridge University Press: New York, 1989.
(19) Snyder, R. G. *J. Chem. Phys.* **1967**, *47*, 1316.
(20) Hagemann, H.; Strauss, H. L.; Snyder, R. G. *Macromolecules* **1987**, *20*, 2810.
(21) West, J. C.; Cooper, S. L. *J. Polym. Sci., Polym. Symp.* **1977**, *60*, 127.
(22) Srichatrapimuk, V. W.; Cooper, S. L. *J. Macromol. Sci., Phys.* **1978**, *B15*, 267.
(23) Coleman, M. M.; Lee, K. H.; Skrovanek, D. J.; Painter, P. C. *Macromolecules* **1986**, *19*, 2149.
(24) Bummer, P. M.; Knutson, K. *Macromolecules* **1990**, *23*, 4357.
(25) Lee, H. S.; Wang, Y. K.; MacKnight, W. J.; Hsu, S. L. *Macromolecules* **1988**, *21*, 270.
(26) Pollack, S. K.; Shen, D. Y.; Hsu, S. L.; Wang, Q.; Stidham, H. D. *Macromolecules* **1989**, *22*, 551.
(27) Shen, D. Y.; Pollack, S. K.; Hsu, S. L. *Macromolecules* **1989**, *22*, 2564.
(28) Pollack, S. K.; Smyth, G.; Papadimitrakopoulos, F.; Stenhouse, P. J.; Hsu, S. L.; MacKnight, W. J. *Macromolecules* **1992**, *25*, 2381.
(29) Gromek, J. M., Institute of Material Science, University of Connecticut, Storrs, CT 06269.
(30) Yoon, S. C.; Snug, Y. K.; Ratner, B. D. *Macromolecules* **1990**, *23*, 4351.
(31) Struik, L. C. E. *Physical Aging in Amorphous Polymers and Other Materials*; Elsevier Science Publishing Co.: New York, 1978.
(32) Wunderlich, B. In *Macromolecular Physics*; Academic Press: New York, 1973–80; Vols. 1–3.
(33) Stenhouse, P. J.; Valles, E. M.; Kantor, S. W.; MacKnight, W. J. *Macromolecules* **1989**, *22*, 1467.
(34) Papadimitrakopoulos, F.; Sawa, E.; MacKnight, W. J., to be published.
(35) Seymour, R. W.; Estes, G. M.; Cooper, S. L. *Macromolecules* **1970**, *3*, 579.
(36) MacKnight, W. J.; Yang, M. *J. Polym. Sci., Polym. Symp.* **1973**, *42*, 817.
(37) Skrovanek, D. J.; Painter, P. C.; Coleman, M. M. *Macromolecules* **1986**, *19*, 699.
(38) Coleman, M. M.; Graf, J. F.; Painter, P. C. *Specific Interactions and the Miscibility of Polymer Blends*; Technomic Publishing Co., Inc.: Lancaster, PA, 1991.
(39) Wang, Q. Master Thesis, University of Massachusetts at Amherst, 1989.
(40) Smyth, G.; Valles, E. M.; Pollack, S. K.; Grebowicz, J.; Stenhouse, P. J.; Hsu, S. L.; MacKnight, W. J. *Macromolecules* **1990**, *23*, 3389.
(41) Maddams, W. F. *Appl. Spectrosc.* **1980**, *34*, 245.
(42) Skrovanek, D. J.; Howe, S. E.; Painter, P. C.; Coleman, M. M. *Macromolecules* **1985**, *18*, 1676.
(43) Brunette, C. M.; Hsu, S. L.; MacKnight, W. J. *Macromolecules* **1982**, *15*, 71.
(44) Senich, G. A.; MacKnight, W. J. *Macromolecules* **1980**, *13*, 106.
(45) Schroeder, L. R.; Cooper, S. L. *J. Appl. Phys.* **1976**, *47*, 4310.
(46) Coleman, M. M.; Skrovanek, D. J.; Howe, S. E.; Painter, P. C. *Macromolecules* **1985**, *18*, 299.
(47) Papadimitrakopoulos, F.; Sawa, E.; MacKnight, W. J., to be published.

Registry No. 2,6-LCPU-6 (copolymer), 117252-65-0; 2,6-LCPU-6 (SRU), 142395-74-2.